

# The Particular Importance of **Galileo E6C**



iStock photo 70357383 by Shaun Wilkinson

Like a pilot boat helping navigate a cargo-laden ship into port, the Galileo E6C pilot signal can lead the E6B data signal component to improved performance.

A research team presents a brief study of the potential performance of a number of processing modes for the Galileo E6 signal, with primary focus on the relative benefits of processing the E6C pilot signal. Experiments center on carrier-phase tracking and data demodulation, providing insight into the utility of the E6 signal both as a communication channel and as a ranging signal. The data recovery from E6B and the availability of E6 carrier-phase measurements are noticeably enhanced when E6C is used for synchronization.

**T**he Galileo E6 signal is centered at 1278.75 MHz, and comprises three signals: an authorized signal (E6A, the publicly regulated service, PRS plus two civilian signals), a data component (E6B), and a pilot component (E6C). Both E6B and C are modulated using binary-phase shift keying (BPSK) code division multiple access (CDMA) memory codes, having lengths of 5,115 chips and chipping rates of 5.115 Mcps.

The pilot signal further employs a secondary code, at a rate of one ksps, with a length of 100 symbols, while the data signal carries symbols at a rate of one ksps, being a half-rate encoded 500-bps message. This distinguishes the Galileo E6B signal as having the highest symbol rate and the highest data rate of any GNSS signal.

As such, it is quite interesting to study the signal in terms of tracking and data delivery performance. To this end, in this article we will first provide a study of the theoretical bounds on processing the E6 signal and, secondly, examine the behavior of current E6-enabled GNSS receivers.

## **Theoretical Bounds**

We begin with an overview of the theoretical performance of a simplified GNSS receiver processing Galileo E6, either as a data-only signal, or as a data-pilot pair. We will examine the carrier-phase tracking and the data-demodulation performance to estimate the relative benefits of processing the pilot signal.

**Carrier Synchronization.** We can characterize carrier-phase tracking in a GNSS

**JAMES CURRAN**  
INDEPENDENT RESEARCHER

**TOR MELGARD**  
FUGRO SATELLITE POSITIONING AS,  
OSLO, NORWAY

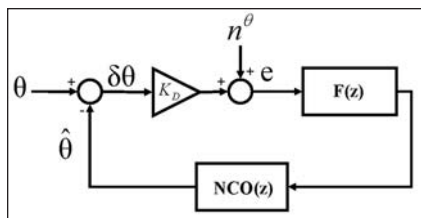


FIGURE 1 Linearized Phase-Domain PLL Model

receiver, when operating in its linear region, by the phase domain model presented in **Figure 1**. Under this model, the effective noise bandwidth of the phase lock loop (PLL) can be estimated from the closed-loop transfer function:

$$H_n(z) = \frac{NCO(z)F(z)}{1 + K_D NCO(z)F(z)}$$

where the PLL filter is denoted by  $F(z)$ , the numerically controlled oscillator is defined by  $NCO(z)$ , typically modelled as an integrator, and the discriminator gain, in rad/rad, is given by  $K_D$ .

From this transfer function, the phase tracking jitter can be predicted as:

$$\sigma_{\delta\theta}^2 = \frac{N_\theta}{2\pi T_L} \int_{-\pi}^{\pi} |H_n(e^{-j\omega})|^2 d\omega$$

where  $N_\theta$  represents the equivalent noise floor after the discriminator, and accounts for the squaring loss that the

nonlinearity of the carrier phase discriminator can induce, such that it increases as the prevailing carrier to noise floor ratio,  $C/N_0$  is reduced.

Both  $K_D$  and  $N_\theta$  depend on the discriminator used in the PLL, and the received signal characteristics generally influence the choice of discriminator. When an unknown data sequence modulates the signal, a Costas-style discriminator is employed, which is insensitive to BPSK modulation, while a pure-PLL discriminator is used when a pilot signal is available.

The tracking performance of PLLs that use either of these discriminators, although similar under nominal conditions, can diverge significantly under weak-signal conditions. In particular, the effective gain of the discriminator diminishes rapidly, and the region of phase errors over which the discriminator provides a proportional response contracts. These two factors can result in sporadic cycle-slips, or loss of lock, when the receiver experiences any appreciable phase dynamic.

In particular, the linear region plays an important role in determining PLL performance. The linear region of an ideal discriminator would extend from  $-\pi$  to  $+\pi$ , for a pure PLL, and from  $-\pi/2$

to  $+\pi/2$ , for a Costas PLL. Although this is achieved under high  $C/N_0$  conditions, under nominal operating conditions, this region is smaller, and contracts as the received signal power reduces, with the onset of this contraction occurring earlier for the Costas PLL.

**Figure 2** depicts the carrier-phase tracking jitter and discriminator linear region for a typical pure-PLL and Costas-PLL for a range of  $C/N_0$ . The curves depict the  $3\sigma$  bound for typical PLL configurations for a receiver processing the Galileo E6B and E6C signals, having a 20-hertz bandwidth and a one-kilohertz loop update rate.

The curves represent a static receiver; so, the estimated  $3\sigma$  bound has been further offset by a phase margin,  $\Delta\theta$ . The latter term reflects any residual stress that the PLL might experience, such as receiver dynamics, oscillator phase noise, or physical vibration and shock. Also included is the estimated linear region of the two classes of PLL discriminator, which can be seen to converge to 180 and 90, respectively, for the pure-PLL (E6C) and for the Costas-PLL (E6B).

These curves offer some insight into the performance that might be observed for a receiver that either processes the Galileo E6B signal alone or employs the pilot signal E6C. In terms of thermal noise-induced phase error, a similar level of tracking error will be observed in either case when the prevailing signal strength is high. As this signal quality reduces below 40 dB-Hz, however, the E6B-only receiver probably will perform more poorly.

We may examine the relative magnitude of the tracking jitter curves and the discriminator linear region in terms of cycle-slippage or loss-of-lock. Specifically, we can observe the phase-margin, or difference between the linear-region and the  $3\sigma$  bound. As this margin is reduced, the probability of the receiver experiencing a cycle-slip increases, and, once the  $3\sigma$  exceeds the linear region, the probability of loss-of-lock is drastically increased.

From **Figure 2** one can surmise that the E6B-only receiver will not be capable

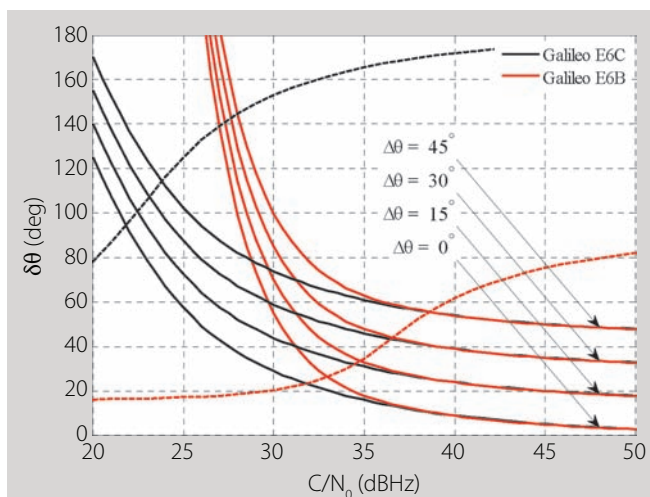


FIGURE 2 The  $3\sigma$  tracking error (solid lines) for the Galileo E6B and E6C signals versus  $C/N_0$  considering a variety of tracking error margins,  $\Delta\theta$ . Note also the linear region of the discriminator used for each signal (broken lines), such that the tracking threshold can be inferred from the point of intersection of the tracking error curve and the discriminator linear region.

of tracking the carrier below approximately 38 dB-Hz, while a receiver that processes E6C might maintain carrier synchronization below 25 dB-Hz. Of course, these figures assume a static receiver, and exclude factors such as receiver motion and multi-path, both of which will bias these results, likely further favoring the E6C case.

### Data Recovery

Depending on how the receiver processes the data signal, E6B, three modes of operation for demodulation of the E6B data are possible: coherent demodulation of each E6B data symbol, the differential demodulation of successive E6B symbols, and the differential demodulation of the E6B symbols relative to the E6C pilot.

For the two E6B-only modes of demodulation, the ultimate performance depends on the level of carrier synchronization that is maintained during the demodulation operation. At the same time, for the differential E6B mode relative to E6C, only the received signal strength plays a role.

For coherent demodulation of each E6B data symbol, carrier-phase alignment must be maintained, keeping the local carrier replica either in phase or in anti-phase, with the received signal rendering the entire signal to the in-phase correlator value,  $I_i^B$ . We can then achieve symbol demodulation by making either a hard- or soft-decision on the sign of this value. Once the receiver identifies a preamble, the polarity of the sequence can be ascertained, and the remainder of the symbols, interpreted. For example, the hard decision may take the form:

$$\hat{a}_i = \text{sign}(I_i^B)$$

where  $\hat{a}_i$  denotes the estimate of the  $i^{\text{th}}$  data symbol, and the superscript,  $B$ , denotes E6B.

For the differential demodulation of successive E6B symbols, the requirements for carrier synchronization are reduced such that the frequency of the received signal and local carrier replica should be equal, but the absolute phase need not be aligned. Assuming that the

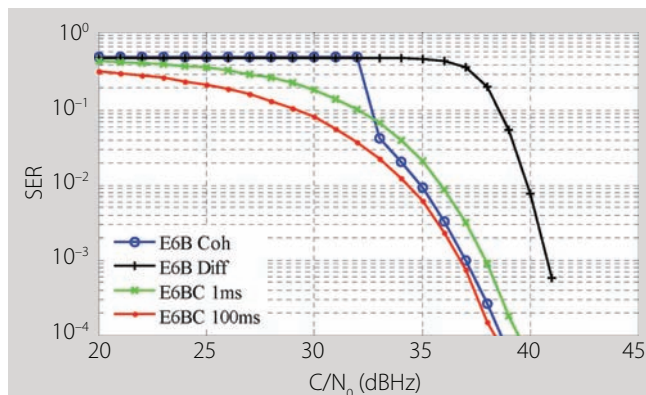


**FIGURE 3** Modified symbol error rate (SER) curves for the E6B signal versus  $C/N_0$  data-only and data-pilot demodulation schemes, including the effects of carrier-phase tracking jitter and tracking threshold on the coherent demodulation, “E6B Coh.”

signals are maintained at an approximately constant but arbitrary phase, a receiver can determine whether two successive symbols are the same, or different, by checking whether the correlator values undergo a phase inversion. Specifically, a receiver may arbitrarily assume that the first symbol is +1 and construct a sequence of symbols relative to this assumption.

The decision as to whether the current symbol is the same as the previous can be expressed as:

$$\hat{c}_i = \text{sign}(I_i^B I_{i-1}^B + Q_i^B Q_{i-1}^B)$$

such that  $-1$  indicates that the successive symbols differ. Again, once a preamble has been identified, the polarity of the entire sequence can be corrected, if necessary. For example, in this case, the hard decision for the  $n^{\text{th}}$  symbol may take the form:

$$\hat{a}_i = \prod_{k=0}^i \hat{c}_k$$

Finally, for the differential demodulation of the E6B symbols relative to E6C, the requirements for carrier synchronization are, again, only that of frequency equality. Assuming that the signals are maintained at an approximately constant arbitrary phase, the absolute sign of the data symbol can be determined by examining the relative phase of the data and pilot component. For example the hard decision for the  $n^{\text{th}}$  symbol may take the form:

$$\hat{a}_i = \text{sign}(I_i^B I_i^C + Q_i^B Q_i^C)$$

where the superscript  $C$  denotes E6C. Note that, although the coherent integration period is limited to one millisecond for E6B, it may be extended significantly for the E6C component.

In terms of data demodulation, **Figure 3** depicts the predicted symbol-error-rate (SER) for a variety of tracking modes versus  $C/N_0$ . Beginning with the most sensitive scheme, the differential demodulation of the data-only channel, the “E6B Diff” curve shows the SER trend of a receiver that operates only on the E6B signal and does not require phase-lock with the signal.

The demodulation scheme, in principle, should provide correct demodulation even in the presence of large phase errors or small frequency errors. However, due to the large number of symbols between each synchronization pattern, or preamble, the scheme is highly sensitive to noise. As a result, it performs the most poorly of the three schemes examined failing to provide any useful information below a  $C/N_0$  of 38 to 40 dB-Hz.

Moving next to the coherent demodulation of the E6B signal, the “E6B Coh” curve shows the SER trend of a receiver that operates only on the E6B signal but which does require phase-lock with the signal. In this case the SER in the moderate- to high- $C/N_0$  region is very close to the theoretical baseband error-rate of  $SER = \frac{1}{2} \text{erfc}(\sqrt{E_b/N_0})$ .

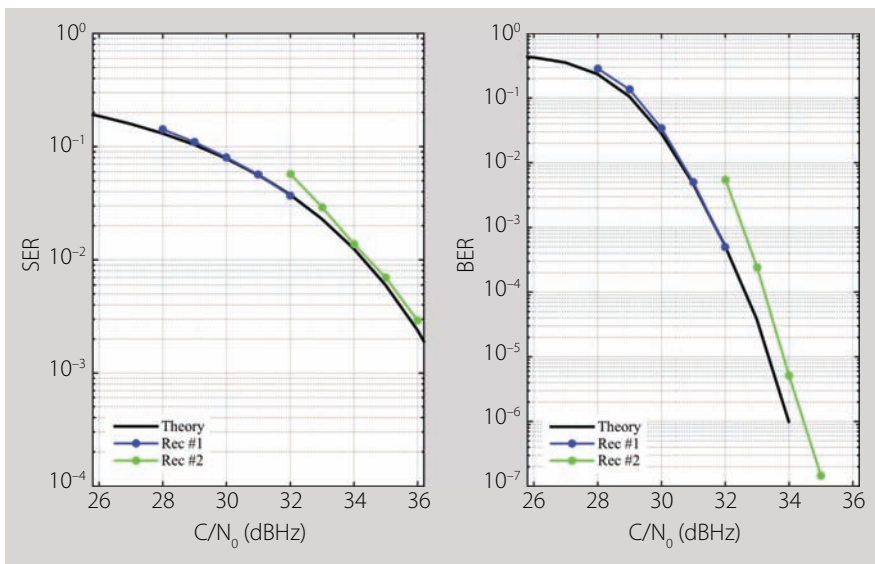


**FIGURE 4** BER curves for the two receivers under test, and the theoretical values. Error rates are unmeasurable for high  $C/N_0$ , and the measured curves tend to zero. For low  $C/N_0$  values the curves are truncated when the receiver no longer provides data.

However, performance is contingent upon the phase error being small. As the  $C/N_0$  is reduced, the nominal phase error grows with the result that the SER increases. Ultimately the receiver will lose lock, resulting in a complete loss of phase-coherence and data extraction. For the receiver configuration assumed in this case, this occurs at a  $C/N_0$  of approximately 33 dB-Hz. Depending on the receiver configuration, this threshold may vary. Within this region, however, the carrier-phase tracking threshold of the receiver determines data availability.

Finally, in Figure 3 the curves “E6BC Diff 1 ms” and “E6BC Diff 100 ms” indicate the differential demodulation of the E6B data signal relative to the E6C pilot signal. In this case, the data is determined by the relative phase of the two signal components and is independent of the absolute phase of the received signal pair. This implies that phase-lock is not required, provided that the frequency error is small relative to the symbol rate.

The difference between these two curves is the coherent integration period applied to the pilot signal, which can be extended arbitrarily. Note that this need not necessarily be the same as that applied by the PLL. Examining the curves, one can see that a moderate SER is maintained even for very low  $C/N_0$

values and that the increase in coherent integration on the pilot signal can yield a SER asymptotically equal to the theoretical best-case.

### Receiver Tests

This section briefly examines the relative operating performance of some receivers processing the Galileo E6BC signals either as a data-pilot pair (E6BC), as a pilot-only signal (E6C), or as a data-only signal (E6B) configuration. The aim is to gain some insight into the data-pilot architecture on E6 can be exploited, how much reliance should be placed on the pilot component, and how well the data signal can be processed in the absence of the pilot signal.

**Data Recovery.** Data recovery performance of the two receiver configurations receivers was assessed using a simulated constellation of signal measurements. A simulation-based test was chosen to ensure repeatability and reliability of the results. An ad-hoc reference scenario was simulated which synthesized signals over a wide range of signal-to-noise ratios — from that which induced moderate to high data loss to that which did not affect data recovery in any way.

The effective  $C/N_0$  observed at the receiver was selected across a range of 25 to 50 dB-Hz, in steps of one decibel. For

each particular  $C/N_0$ , the interference was first omitted, allowing the receiver to acquire the satellite signals, and subsequently introduced at a fixed power. We then collected navigation symbols in sets of 1,000 symbols according to the prevailing  $C/N_0$  and used these to compute the effective BER. **Figure 4** presents the results of these tests, providing the measured SER, equivalent BER and theoretical curves.

The measured results show reasonably good agreement with the theoretical model over the regions for which BER curves can be computed. In **Figure 4**, these regions are bounded on the right-hand-side by the limited observation time, which makes it difficult to observe very low error rates, and on the left-hand-side when the receiver fails to provide navigation data.

Examining the results, the receiver that only processes the data signal clearly fails to provide data measurements below a  $C/N_0$  of approximately 33 dB-Hz. At this point, the receiver appears to have lost lock on the signal. In contrast, with the aid of the pilot signal, the other receiver continues to provide data, albeit with an increasing error rates. One further observation that we can make is that the curve representing the BER for receiver number two exceeds that which would be expected, whereas that of receiver number one does not. This observation aligns with the notion that the onset of carrier tracking problems influences the data recovery performance more for non-pilot aided receivers

**Measurement Quality & Availability.** To assess the effect of the pilot signal on the availability and quality of the positioning observables, we conducted a zero-baseline test. A roof-mounted GNSS antenna connected to an RF splitter provided an un-attenuated feed to a reference receiver and, via an adjustable attenuator, to the two receivers under test.

Using this configuration, we logged a precise set of observations from the reference receiver, while measurements from the receivers under test were logged for a range of controlled  $C/N_0$

conditions. One of the receivers under test was configured to perform data-only tracking of Galileo E6B, while both the second and reference receiver, were configured to perform data-pilot tracking of Galileo E6BC.

The test was conducted on when two Galileo satellites were visible to the reference antenna at elevations of greater than 45 degrees and at  $C/N_0$  greater than 50 dB-Hz. Measurements, including  $C/N_0$ , carrier-phase, and pseudorange were logged at one hertz over a period of one hour. During this time the attenuator provided a controlled reduction in received signal-strength, from 0 to 30 decibels. The upper subplot of Figure 5 shows the average observed  $C/N_0$  for the two satellites. The reference receiver observed  $C/N_0$  of approximately 50 dB-Hz on both satellites throughout the test.

Zero-baseline double-difference pseudorange, denoted here by  $\Delta^2\rho$ , and carrier phase, denoted here by  $\Delta^2\theta$ , measurements were then computed to ascertain what influence the availability of the pilot signal has on the measurement quality. The double-difference between the reference receiver and each of the receivers under test is shown in the second and third subplots of Figure 5, which depicts the three-sigma computed over two minute windows. In this case, as the three receivers were connected to the same antenna, the magnitude of the double-difference should be representative of the thermal noise contribution to the measurements which, in this case, is dominated by the noise of the receiver processing the attenuated signal.

In terms of availability, the two receivers clearly behave differently under weak-signal conditions, with the data-only receiver (number two) failing to provide pseudorange and carrier-phase measurements below 37 and 35 dB-Hz, respectively. In contrast, receiver number one, which processes the pilot signal, can provide relatively accurate measurements to a  $C/N_0$  of approximately 25 dB-Hz. In terms of carrier phase measurement quality, at high  $C/N_0$  the receivers exhibit a similar level of thermal noise-induced error; however, as

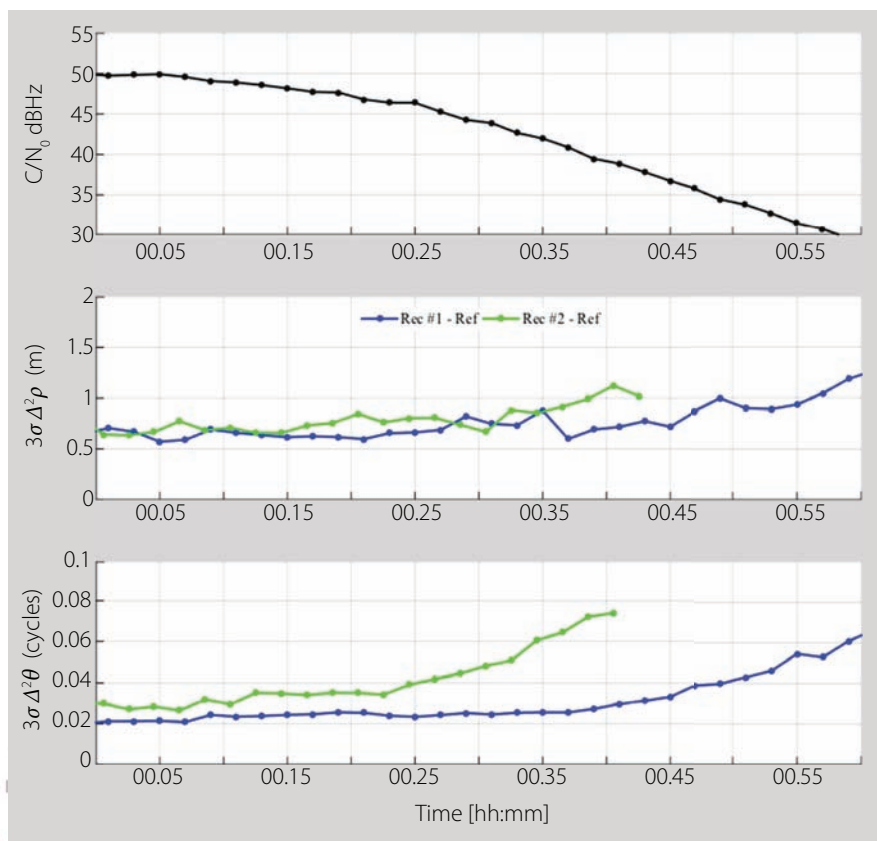


FIGURE 5 Zero-baseline double-difference carrier phase and pseudorange measurements for Galileo E6 as a function of received signal  $C/N_0$ .

the signal strength is reduced, the error increases more rapidly for receiver number two, showing good agreement with the theoretical results of Figure 2.

### Positioning and Benefits of E6

In the positioning domain, the Galileo E6 signal provides an independent pseudorange that can be beneficial during interference in the E1 band. However, our focus here is on carrier-phase ambiguity resolution for long baselines and for precise point positioning (PPP), where ionospheric effects can be largely unknown. High-end user applications are assumed, which would typically involve receivers capable of tracking all available signals. The subsequent analysis focuses in particular on the contribution of the E6 carrier phase.

Triple-frequency GNSS may enable both rapid and reliable ambiguity resolution for long baseline, real-time kinematic (RTK) positioning. The use of more signals from each GNSS satel-

lite improves time-to-first-fix (TTFF). For instance, triple-frequency RTK has been shown to give a considerably higher success rate than dual-frequency. Three-carrier ambiguity resolution can always be achieved by direct application of the least-squares ambiguity decorrelation adjustment (LAMBDA).

We can also find certain linear combinations for Galileo, using both carrier phase and code measurements, so that the speed and reliability of ambiguity fixing can be improved. Such combinations frequently involve the use of the E6 carrier phase. The trade-off, however, is that the noise of these combinations is much higher than the original carrier-phase measurement noise. The target here is to give qualitative statements about the expected performance when using, for instance, the LAMBDA method on specific dual-, triple-, and quadruple-frequency Galileo signals.

A simplified model of the phase observation including the ionospheric

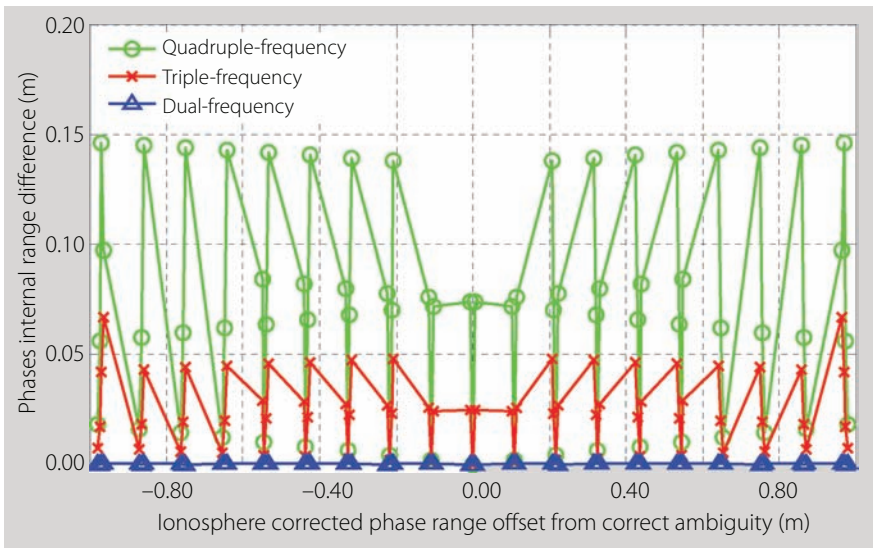


**FIGURE 6** Simulation for single-, dual-, triple-, and quadruple-frequency Galileo carrier phase ranges where the E1 ionosphere is considered unknown within +/-1 m.

effect can be written as:

$$L_F = \rho - \frac{K}{f_F^2} + \lambda_F N_F + \varepsilon_F.$$

Tropospheric delay, receiver and satellite clock errors, and phase biases are considered known and are not shown.  $\rho$  is the geometric distance,

$$\frac{K}{f_F^2}$$

is the slant ionospheric delay at frequency  $f_F$ ,  $\lambda_F N_F$  is the phase ambiguity, where  $\lambda_F$  is the wavelength at frequency  $f_F$  and  $N_F$  is the integer ambiguity, and  $\varepsilon_F$  includes the unmodeled effects, such as measurement noise and multipath.

Full phase alignment for triple-frequency measurements  $L_1$ ,  $L_2$ , and  $L_3$  is achieved when  $L_1 = L_2 = L_3$ , which, when setting the unmodeled effects to zero, gives:

$$\lambda_1 N_1 - \frac{K}{f_1^2} = \lambda_2 N_2 - \frac{K}{f_2^2} = \lambda_3 N_3 - K f_3^2$$

for which the phases' internal range difference  $\Delta L_{Max}$  is zero and thus  $\Delta L_{Max} = 0$ , where  $\Delta L_{Max} = \max(|L_1 - L_2|, |L_1 - L_3|)$ .

**Figure 6** shows a simulation for Galileo when the ionosphere is considered unknown within plus/minus one meter at the E1 frequency. The internal range differences are displayed as a function of phase range, and the horizontal axis shows the phase range in meters around

the correct range at zero. At the correct range, and in the absence of thermal noise and multipath,  $\Delta L_{Max}$  is zero. The figure shows how the different phase ranges agree at a given range.

The simulation, based on the principle of cycling through possible phase ambiguities for the first two carrier-phase signals and calculating the ionosphere correction, provides phase alignment. This ionosphere is then applied to all phase measurements. The vertical axis illustrates how well the phase alignment  $\Delta L_{Max}$  can be used to separate the correct ambiguity from the other candidates. The higher  $\Delta L_{Max}$  is for the erroneous candidates, the greater the chance of selecting the ambiguities pointing to the correct range.

Dual-frequency provides relatively poor performance, as then there is no redundancy in the ionosphere observations, so, all candidates are zero on the y-axis. Thus, we can see how triple-frequency, using the E5a-E5b-E1 signals, introduces some redundancy and, consequently, provides improved performance and increased separation from the other ambiguity candidates. However, introduction of the fourth frequency, E6, drastically improves this separation.

With four-frequency Galileo signals, about two-thirds of the ambiguity

candidates can be eliminated based on an internal phase range comparison. Interestingly, separate studies show that a triple-frequency Galileo solution, using E1-E5ab-E6, provides similar performance to that of the quadruple-frequency case shown in Figure 6.

**Conclusion**

Although it is already generally accepted that the use of a pilot signal can significantly improve the accuracy and availability of GNSS ranging measurements, this article has examined the specific case of the Galileo E6BC signals. Having a particularly high symbol rate, the E6B signal is more sensitive than most to the degradation in the received signal quality. The availability of its companion pilot signal, E6C, is important.

Unlike its E1 or E5a counterparts, which have 4- and 20-millisecond symbol periods, respectively, the E6B signal has a very limited capacity for correlation gain. As such, although it might be reasonable to process the E1B or E5aI signals in isolation, it proves more of a challenge to do so for the E6B signal. Indeed, our work has demonstrated, both via theoretical modeling and tests using receivers, that the use of the E6C pilot signal can provide meaningful improvements to receiver performance.

In terms of data extraction on the E6B data signal, the use of the E6C pilot signal for synchronization can provide a noticeably reduced symbol-error-rate and a correspondingly increased availability of the E6 navigation message. As for carrier-phase positioning, the E6C pilot signal appears to improve both measurement availability and measurement accuracy. This improvement in measurement accuracy, extends further to the performance of RTK solutions. Adding the Galileo E6 signal clearly provides significant benefits with respect to carrier-phase ambiguity resolution when ionospheric effects are considered largely unknown.

It is also noteworthy that the observations made here have considered a relatively benign scenario. First, the experiments have considered a static

scenario. In a practical usage case, which would include receiver motion, the carrier synchronization would be stressed. This is likely to elicit a further disparity between the data-only and the data-pilot tracking of the signal, both in terms of data and ranging capability.

Second, the experiments have considered only the case of thermal noise, both in the theoretical model and in the attenuation of the live GNSS signals. In reality, the spectrum in the vicinity of the E6 signals is frequently occupied by moderate to high power telecommunication transmissions, including analog and digital video broadcast, such as DVB-S. These signals can cause a significant degradation to the received GNSS signal quality. In such cases, the increased integration period offered by the pilot signal and the improved isolation offered by the secondary code can be of considerable benefit.

In summary, the Galileo E6C signal seems to serve an important dual purpose: as a facilitator for the use of the data-services carried by its accompanying E6B signal and as an enabler for quadruple-frequency carrier-phase positioning, a unique feature of Galileo.

### Manufacturers

The GNSS simulator used in the tests described in this article was the GSS8000 from **Spirent Communications**, Paignton, United Kingdom. The GPS splitters and attenuator were from **Mini-Circuits**, Brooklyn, New York USA. Identification of the GNSS receivers has been withheld under the terms of a non-disclosure agreement with the researchers.

### Additional Resources

- [1] Cocard, M., and S. Bourgon, O. Kamali and P. Collins, "A Systematic Investigation of Optimal Carrier-Phase Combinations for Modernized Triple-Frequency GPS," *Journal of Geodesy*, Volume: 82, pp. 555-564, 2008
- [2] Curran, J. T., and D. Borio, G. Lachapelle, and C. C. Murphy, "Reducing Front-End Bandwidth May Improve Digital GNSS Receiver Performance," *IEEE Transactions on Signal Processing*, Volume: 58, Issue: 4, pp. 2399-2404, April 2010
- [3] Curran, J. T., and G. Lachapelle and C. C. Murphy, "Improving the Design of Frequency Lock Loops for

GNSS Receivers," *IEEE Transactions on Aerospace and Electronic Systems*, Volume: 48, Issue: 1, pp. 850-868, January 2012

- [4] Geng, G. and Y. Bock, "Triple-Frequency GPS Precise Point Positioning with Rapid Ambiguity Resolution," *Journal of Geodesy*, Volume: 87, Issue: 5, pp. 449-460, 2013 with erratum 2014
- [5] Goldstein, D. B., and J. W. Betz, "Candidate Designs for an Additional Civil Signal in GPS Spectral Bands," *Proceedings of ION-GNSS-2002*, September 2002
- [6] Hagmann, W. and J. Habermann, "On the Phase Error Distribution of an Open Loop Phase Estimator," *Communications (ICC '88)*, Volume: 2, pp. 1031-1037, June 1988
- [7] Henkel, P., and C. Günther, "Reliable Integer Ambiguity Resolution: Multi-Frequency Code Carrier Linear Combinations and Statistical A Priori Knowledge of Attitude," *Journal of the Institute of Navigation*, Volume 59, Issue 1, pp. 61-75, 2012
- [8] Javad, Delta 3, <<https://www.javad.com/jgnss/products/receivers/delta-3.html>>, [Accessed: 01 Feb 2015]
- [9] Julien, O., "Carrier-Phase Tracking of Future Data/Pilot Signals," *Proceedings of ION GNSS 2005*, September 2005
- [10] Kaplan, E. D., ed., *Understanding GPS: Principles and Applications*, Volume 1, Chapter 5, pp. 179-194, Artech House, Inc., 2006, ISBN 1-58053-894-0
- [11] O'Keefe, K., and O. Julien, M. E. Cannon and G. Lachapelle, "Availability, Accuracy, Reliability, and Carrier-Phase Ambiguity Resolution with Galileo and GPS," *Acta Astronautica*, Volume: 58, Issue: 8, pp. 422-434, 2006
- [12] Odijk, D., and B. Arora and P. Teunissen, "Predicting the Success Rate of Long-baseline GPS+Galileo (Partial) Ambiguity Resolution," *Journal of Navigation*, Volume: 67, Issue: 3, pp. 385-401, 2014
- [13] Proakis, J. G., *Digital Communications, Electrical Engineering Series*, McGraw Hill International Editions, 3rd ed., 1995, ISBN 0-07-232111-3
- [14] Sauer, K., and U. Vollath and F. Amarillo, "Three and Four carriers for Reliable Ambiguity Resolution," *Proceedings of ENC GNSS, 2004*
- [15] Septentrio, AsteRx-U. <<http://www.septentrio.com/products/gnss-receivers/rover-base-receivers/integrated-gnss-receivers/asterx-u->>, [Accessed: 01 Feb 2015]
- [16] Stephens, S. A., and J. B. Thomas, "Controlled Root Formulation for Digital Phaselocked Loops," *IEEE Transactions on Aerospace and Electronic Systems*, Volume: 31, Issue: 1, pp. 78-95, January 1995
- [17] Teunissen, P. J. G., "The Least-Squares Ambiguity Decorrelation Adjustment: A Method for Fast GPS Integer Ambiguity Estimation," *Journal of Geodesy*, Volume: 70, pp. 65-82, 1995
- [18] Topcon, NetG5. <[https://www.topconpositioning.com/sites/default/files/product\\_files/netg5\\_broch\\_7010\\_2145\\_rev\\_c\\_sm.pdf](https://www.topconpositioning.com/sites/default/files/product_files/netg5_broch_7010_2145_rev_c_sm.pdf)>, [Accessed: 01 Feb 2015]

[19] Trimble, NetR9 <<http://www.trimble.com/Infrastructure/Trimble-NetR9.aspx>>, [Accessed: 01 Feb 2015]

[20] VanDierendonck, A. J., *Global Positioning System: Theory & Applications*, Volume One, Progress in Astronautics and Aeronautics, Chapter 8, pp. 329-408, AIAA, 1996

[21] Vollath, U., and K. Sauer, F. Amarillo and J. Pereira, "Three or Four Carriers – How Many are Enough?," *Proceedings of ION GNSS 2003*, 2003

[22] Winkel, J. O., *Spreading Codes for a Satellite Navigation System*, October 11 2011, US Patent 8,035,555

[23] Zhuang, W., "Performance Analysis of GPS Carrier Phase Observable," *IEEE Transactions on Aerospace and Electronic Systems*, Volume: 32, Issue: 2, pp. 754-767, April 1996

### Authors



**James T. Curran** received a B.E. in electrical & electronic engineering and a Ph.D. in telecommunications from the Department of Electrical Engineering, University College Cork, Ireland. He worked as a research engineer with the PLAN Group in the University of Calgary, Canada, as a grant-holder at the Joint Research Center, Italy. He has recently joined SERCO, working as a radionavigation engineer at the European Space Agency, in Noordwijk, the Netherlands.



**Tor Melgard** is senior scientist at Fugro Satellite Positioning in Oslo. He received a Ph.D. in geomatics engineering at the University of Calgary (Canada). He has an M.Sc. in electrical engineering

from the Norwegian Institute of Technology and he has worked in the field of satellite navigation since 1993. 